Journal of Energy Chemistry 42 (2020) 180–184

Contents lists available at ScienceDirect

Journal of Energy Chemistry

journal homepage: www.elsevier.com/locate/jechem

http://www.journals.elsevier.com/journal-of-energy-chemistry/

Communication

Dual-ion hybrid supercapacitor: Integration of Li-ion hybrid supercapacitor and dual-ion battery realized by porous graphitic carbon

Changzhen Zhan[a], Xiaojie Zeng[a], Xiaolong Ren[a], Yang Shen[a,*], Ruitao Lv[a], Feiyu Kang[b,c], Zheng-Hong Huang[a,b,**]

[a] State Key Laboratory of New Ceramics and Fine Processing, School of Materials Science and Engineering, Tsinghua University, Beijing 100084, China
[b] Key Laboratory of Advanced Materials (MOE), School of Materials Science and Engineering, Tsinghua University, Beijing 100084, China
[c] Engineering Laboratory for Functionalized Carbon Materials, Graduate School at Shenzhen, Tsinghua University, Shenzhen 518055, China

ARTICLE INFO

Article history:
Received 7 April 2019
Revised 18 May 2019
Accepted 3 June 2019
Available online 13 July 2019

Keywords:
Dual-ion hybrid supercapacitor
Hybrid supercapacitor
Lithium-ion battery
Dual-ion battery
Porous graphitic carbon
Hybrid mechanism

ABSTRACT

Lithium-ion hybrid supercapacitors (Li-HSCs) and dual-ion batteries (DIBs) are two types of energy storage devices that have attracted extensive research interest in recent years. Li-HSCs and DIBs have similarities in device structure, tendency for ion migration, and energy storage mechanisms at the negative electrode. However, these devices have differences in energy storage mechanisms and working potentials at the positive electrode. Here, we first realize the integration of a Li-HSC and a DIB to form a dual-ion hybrid supercapacitor (DIHSC), by employing mesocarbon microbead (MCMB)-based porous graphitic carbon (PGC) with a partially graphitized structure and porous structure as a positive electrode material. The MCMB-PGC-based DIHSC exhibits a novel dual-ion battery-capacitor hybrid mechanism: it exhibits excellent electronic double-layer capacitor (EDLC) behavior like a Li-HSC in the low-middle wide potential range and anion intercalation/de-intercalation behavior like a DIB in the high-potential range. Two types of mechanisms are observed in the electrochemical characterization process, and the energy density of the new DIHSC is significantly increased.

Lithium-ion hybrid supercapacitors (Li-HSC), as a combination of lithium ion battery (LIB) and supercapacitor (SC), are novel devices with the advantages of both LIB and SC, and have attracted worldwide attention in recent years [1–4]. During the charging process, the cations (Li^+) in the electrolyte migrate to the negative electrode, driven by the electric field, and finally undergo a Faraday reaction with the negative electrode material. While the anions in the electrolyte migrate to the positive electrode of the capacitor and are finally adsorbed onto the surface of the porous positive electrode material, they form an electronic double-layer structure to realize energy storage [5]. This is different from a LIB; the concentration of ions in the electrolyte in a Li-HSC is constantly changing (decrease during charging and increase during discharging) [6]. The internal ion motion process of Li-HSC is very similar to that of a dual-ion battery (DIB) [7,8]. The differences between a Li-HSC and a DIB are two: (1) The reaction mechanism at the positive electrode. In a DIB, anions undergo an intercalation/de-intercalation reaction into the positive electrode material, which requires the positive electrode to possess a crystalline layered structure, namely a high graphitization degree for a carbon-based material [9]. On the other hand, in a Li-HSC, anions undergo a physical adsorption/desorption reaction on the surface of the positive electrode material to form an electronic double-layer capacitor (EDLC), which requires the positive electrode material to have a highly porous structure [5,10]; (2) The potential of the positive electrode reaction. The intercalation/de-intercalation reaction in a DIB occurs at the high-potential range (4.0–5.0 V vs. Li/Li^+) [11], while the EDLC behavior without Faraday reaction in the positive material occurs at a wide potential range [12].

The difference of the energy storage mechanism and potential range of the positive electrode in DIBs and Li-HSCs provides the possibility of combining a DIB and a Li-HSC. However, realizing a hybrid of DIB and Li-HSC is challenging because of the positive electrode material. The graphitization degree of the positive material is the critical parameter in a DIB. A higher crystallinity leads

* Corresponding author.
** Corresponding author at State Key Laboratory of New Ceramics and Fine Processing, School of Materials Science and Engineering, Tsinghua University, Beijing 100084, China.
E-mail addresses: shyang_mse@mail.tsinghua.edu.cn (Y. Shen), zhhuang@tsinghua.edu.cn (Z.-H. Huang).

https://doi.org/10.1016/j.jechem.2019.06.009

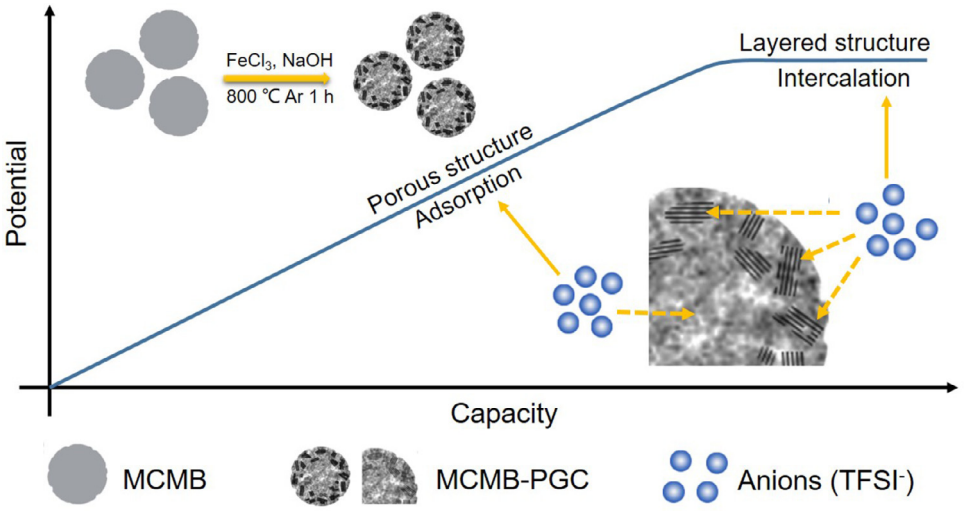

Fig. 1. Schematic diagram of the synthesis of MCMB-PGC and the dual-ion hybrid supercapacitor energy storage mechanism. Here MCMB denotes mesocarbon microbeads and PGC denotes porous graphitic carbon.

to a higher capacity during the anion intercalation/de-intercalation progress [8]. However, it is difficult to construct this porous structure for crystallized graphitic carbon with a high specific surface area (SSA), which is very important for the EDLC behavior in a Li-HSC positive electrode [13]. Hence, carbon material with both a crystallized graphite structure and well developed pore structure is crucial for realizing the combination of a DIB and a Li-HSC. In our previous work, we have systematically studied porous graphitic carbon (PGC), which could possess a partially graphitized structure without the loss of its porosity [14,15]. In this work, we synthesized PGC through a one-step activation/catalytic graphitization route and employed it as the positive electrode material. The PGC positive-electrode material was used to yield the unprecedented integration of a Li-HSC and a DIB, namely, a dual-ion hybrid supercapacitor (DIHSC), which exhibits good EDLC behavior at the low-middle wide potential range as a Li-HSC, and provides some additional plateau capacity at the high-potential range (4.0–5.0 V vs. Li/Li^+) as a DIB. Two different types of mechanisms can clearly be observed in the electrochemical characterization process, and the energy density of the DIHSC is effectively increased by the hybrid energy storage mechanism.

PGC was synthesized through a one-step activation/catalytic graphitization of mesocarbon microbeads (MCMB) by our previous method [14]. Specifically, 0.5 g of MCMB powder was mixed with 2 g of NaOH and 0.075 g of $FeCl_3$ in an agate mortar. The mixture was ground thoroughly and then placed in a tube furnace in a nickel boat. The mixture was calcined at 800 °C (heating rate 5 °C/min) for 1 h under an Ar atmosphere. After cooling to room temperature, the sample was washed with 100 mL of a 1 M HCl solution to remove inorganic impurities, and then was washed thoroughly with deionized water repeatedly until the pH reached 7. The resultant sample was dried in an oven at 120 °C for 24 h and was used as MCMB-PGC. The control sample MCMB-PC was obtained by the same heat treatment and subsequent rinsing process; however, it was $FeCl_3$-free.

Morphologies, structural features, and surface chemistry of MCMB-PGC and the control samples were characterized by scanning electron microscopy (SEM LEO1530), transmission electron microscopy (TEM JEM-2010), X-ray diffraction (XRD, Bruker D8 ADVANCED, 40 kV), and X-ray photoelectron spectroscopy (XPS, PHI Quantera Imaging). The SSA of the carbon materials was calculated by the Brunauer–Emmett–Teller (BET) method using the N_2 sorption isotherms measured at 77 K, and the pore-size distribution (PSD) was calculated by the density functional theory (DFT).

The electrode slurry was obtained by mixing 75% active material, 15% PVDF, and 10% conductive carbon black with N-Methyl pyrrolidone (NMP). The slurry was then coated onto aluminum foil and dried at 120 °C for 12 h in vacuum. The coated aluminum foil was punched into 12 mm plates, and the mass loading of active material on each piece was about 2 mg. All electrochemical tests were conducted using CR2032 coin cells. All CR2032 cells were assembled by an active material electrode and a lithium metal electrode with 1 M bis(trifluoromethylsulfonyl)amine lithium salt (Li-TFSI) in 1–butyl–3-methylimidazolium bis(trifluoromethylsulfonyl)imide (BMIm-TFSI) ionic liquid electrolyte in an Ar glove box.

Galvanostatic charge/discharge (GCD) of the devices was tested by an Arbin-BT2000 test station. The cyclic voltammetry (CV) was conducted using a VSP-300 electrochemical analyzer.

The synthesis process of MCMB-PGC and the energy storage mechanism of a DIHSC are illustrated in Fig. 1. The coexistence of a graphitic structure and porous microstructure in one carbon material is the key factor in realizing the dual-ion energy storage mechanism.

Crystallinity was analyzed by XRD and high resolution transmission electron microscopy (HRTEM). XRD patterns of as-prepared MCMB-PGC and the control sample of MCMB-PC are shown in Fig. 2(a). MCMB-PC exhibits a typical pattern of amorphous carbon with a broad peak at about 43°, corresponding to the (100) disordered carbon layers [16]. The XRD scan of the MCMB-PGC presents two additional sharp peaks at 26.4° and 43.7° in addition to the broad peak appearing in MCMB-PC. The two sharp peaks can be ascribed to the (002) and (100) planes of the highly crystalline carbon layers [14], suggesting that a partial graphite structure was successfully introduced by the catalytic graphitization process; this is further verified by the HRTEM images shown in Fig. 2(b). Amorphous regions and crystalline structure regions with obvious lattice fringes are observed, indicating the partial graphitic structure of MCMB-PGC, which is consistent with the results of our previous work [14]. Such a partial graphitic structure can effectively form a conductive network and dramatically increase the power performance during the EDLC behavior in the low-middle potential range. Moreover, owing to this structure, MCMB-PGC may store energy by serving as a host material for anions and may provide some additional plateau capacity in the high-potential range. Fig. 2(c) shows an SEM image of

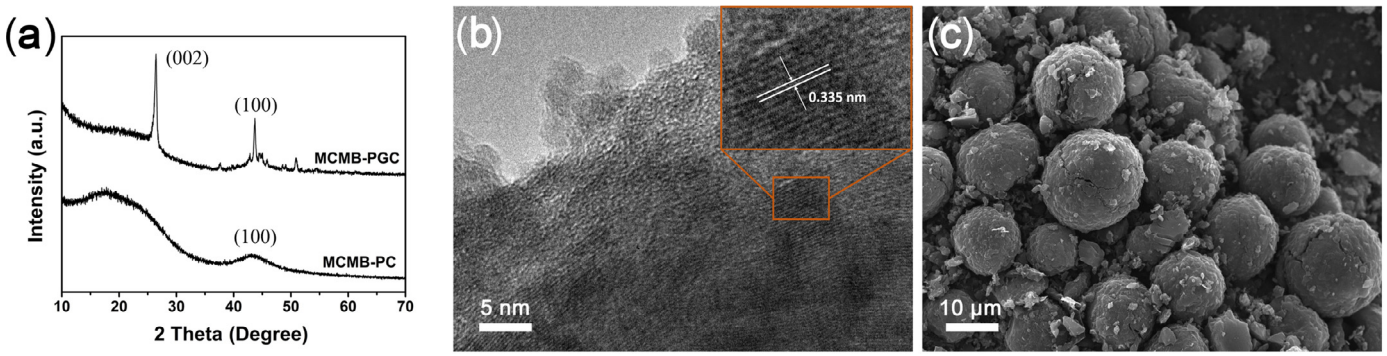

Fig. 2. (a) XRD patterns of as-prepared MCMB-PGC and a control sample of MCMB-PC; (b) HRTEM image of MCMB-PGC; (c) SEM image of MCMB-PGC. Here MCMB-PC denotes MCMB-based porous carbon.

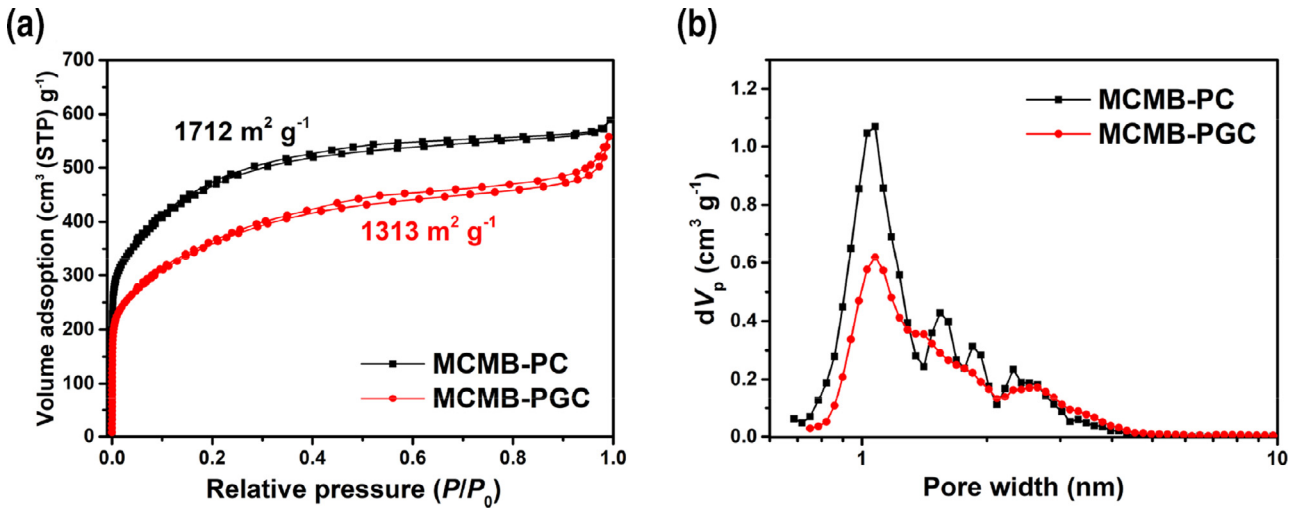

Fig. 3. (a) N_2 adsorption/desorption isotherms and the corresponding (b) pore-size distributions of MCMB-PC and MCMB-PGC.

Table 1. Specific capacity and energy density of MCMB-PC and MCMB-PGC in different potential ranges.

	Specific capacity (1.0 – 5.0 V, mAh g^{-1})	Specific capacity (4.0 – 5.0 V, mAh g^{-1})	Specific capacity (1.0 – 4.0 V, mAh g^{-1})	Energy density (1.0 – 5.0 V, Wh kg^{-1})
MCMB-PC	186.1	4.2	181.9	398
MCMB-PGC	204.2	22.9	181.3	581
Difference (%)	+9.7	+445.2	−0.3	+46.0

Calculated by galvanostatic discharge results, based on the mass of active material on the positive material.

MCMB-PGC. The spherical shape of MCMB with diameters of about 20–40 μm was well maintained during the one-step activation/catalytic graphitization process.

N_2 adsorption/desorption conducted at 77 K was also used to investigate the porosity of MCMB-PGC, which contributes to its EDLC performance. The N_2 adsorption/desorption isotherms of MCMB-PGC and MCMB-PC are shown in Fig. 3(a). Both of them show hybrid sorption isotherms of type I and type IV with an H4 hysteresis loop [17]. The sharp sorption increase in the low relative pressure was attributed to the abundant micropores, and the hysteresis loop revealed the existence of mesopores [18]. However, MCMB-PGC exhibits a lower nitrogen uptake than MCMB-PC, which is ascribed to the destruction of porous structure of the disordered amorphous carbon and the formation of dense graphitic carbon around the surface of iron catalyst during the high-temperature heat treatment process [19,20]. As a result, the SSA calculated by the BET method also decreased from 1712 m^2 g^{-1} for MCMB-PC to 1313 m^2 g^{-1} for MCMB-PGC. The PSD curves calculated by the DFT method are shown in Fig. 3(b). Both MCMB-PGC and MCMB-PC exhibit multimodal distributions with abundant micropores and moderate mesopores. Such an optimized hierarchical pore structure could provide a large number of energy storage sites and a sufficient high-speed ion transport path, indicating good capacitive performance as EDLC electrode material [21,22].

To further investigate the realization of the integration of a Li-HSC and DIB, electrochemical performance of MCMB-PGC and the control samples were studied, with results shown in Fig. 4 and Table 1. Fig. 4(a) shows the 0.1 A g^{-1} GCD curves of cells assembled with lithium metal and artificial graphite (AG, D50: 23 μm), activated carbon (AC, YP-17D, SSA: 1460 m^2 g^{-1}), a mixture of AG and AC (mass ratio m_{AG}:m_{AC} = 3:7), and the calculated curve by weighted average of AG and AC ($0.3^*Q_{AG} + 0.7^*Q_{AC}$). The AG-based DIB exhibits a typical plateau capacity in the 4.5–5.0 V range during charging, and 4.0–4.5 V during discharging, corresponding with the intercalation/de-intercalation process of the anions. The AC-based Li-HSC exhibited a linear curve due to the EDLC behavior of anions on the surface of the electrode material. Both of the curve shapes and capacities of the mixture of AG and AC-based half-cells are nearly coincident with the result calculated by the

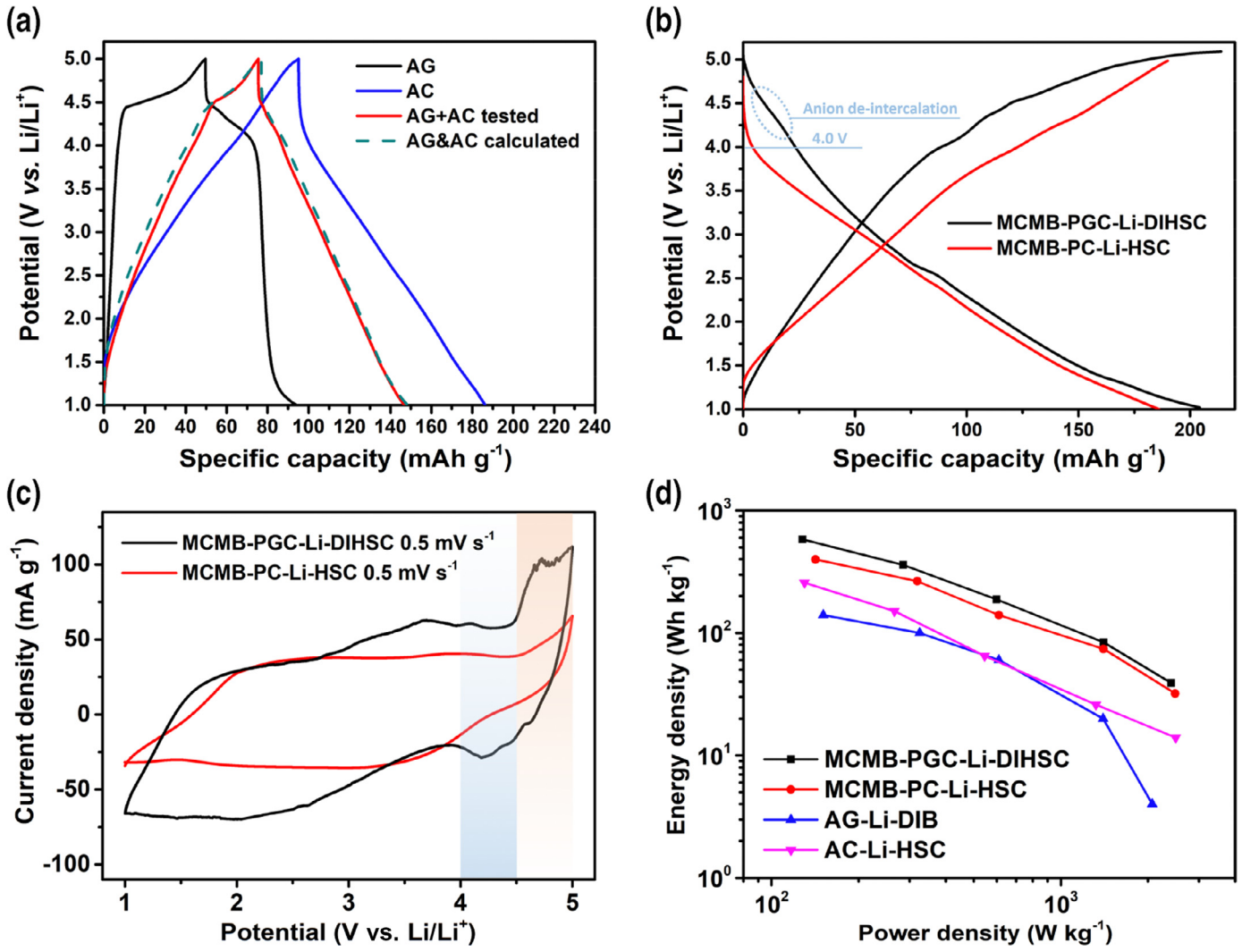

Fig. 4. (a) GCD curves of AG, AC, a mixture of AG and AC, and the calculated curve by weighted average under 0.1 A g^{-1}; (b) GCD curves of a MCMB-PGC-based Li-DIHSC and a MCMB-PC-based Li-HSC under 0.1 A g^{-1}; (c) CV curves of MCMB-PGC-based Li-DIHSC and MCMB-PC-based Li-HSC under 0.5 mV s^{-1}; (d) Ragone plots of the as-fabricated devices. Here AG denotes artificial graphite; AC denotes activated carbon; HSC denotes hybrid supercapacitor; DIB denotes dual-ion battery; DIHSC denotes dual-ion hybrid supercapacitor.

weighted average. This reveals that there is little synergistic effect of AC and AG in their mechanical mixture, and that direct mixing of crystalline carbon and porous carbon is not an effective strategy to realize the DIHSC. Fig. 4(b) shows the charge and discharge curves of a MCMB-PGC-based Li-DIHSC and a MCMB-PC-based Li-HSC under 0.1 A g^{-1}. In the low-middle potential range (1.0–4.0 V vs. Li/Li^+), both MCMB-PC and MCMB-PGC exhibit linear discharge curves and much higher specific capacity than AC (in Fig. 4a), which is ascribed to the sufficient SSA and optimized hierarchical pore structure of MCMB-PC and MCMB-PGC. Moreover, the two discharge curves are almost parallel and the specific capacities contributed at 1.0–4.0 V (shown in Table 1) are nearly equal, indicating that the good EDLC behavior led by the porous structure is well maintained in MCMB-PGC.

In the high potential range (4.0–5.0 V vs. Li/Li^+), MCMB-PGC shows a nearly 5.5 times higher discharge specific capacity than MCMB-PC (see Table 1). The performance enhancement at high potential can be attributed to the following two aspects: (1) The partial graphitic structure significantly enhances the electrical conductivity of the material, thereby reducing the IR drop and the performance loss caused by the internal resistance. (2) The graphitic part of the PGC provides some additional plateau capacity by means of the de-intercalation of anions. The combination of two different types of mechanisms can be further observed in the CV curves shown in Fig. 4(c). One can see that the MCMB-PC exhibits a quasi-rectangular shaped CV curve. However, MCMB-PGC presents a pair of additional broad redox peaks at 4.5–5.0 V and 4.0–4.5 V, corresponding to the intercalation/de-intercalation of anions in the graphitic layers, respectively. Because this capacity increase occurs at a high potential range (4.0–5.0 V), it can significantly enhance the energy density of the device while employed as positive electrode material. In order to investigate the energy performance enhancement of the dual-ion battery-capacitor hybrid mechanism more directly, Ragone plots (energy density vs. power density, calculated from the mass of active material on the positive material) of the devices are summarized in Fig. 4(d). One can see MCMB-PGC-based Li-DIHSC exhibits an extremely high energy density of 581 W h kg^{-1}, which is much higher than the 398 W h kg^{-1} displayed by MCMB-PC-based Li-HSC, the 257 W h kg^{-1} by AC-based Li-HSC, and the 141 W h kg^{-1} by AG-based DIB, verifying the great performance enhancement of the dual-ion battery-capacitor hybrid mechanism

A novel dual-ion hybrid supercapacitor, namely the integration of a Li-ion hybrid supercapacitor and a dual-ion battery, was

realized by employing MCMB-based PGC as the positive electrode material. The MCMB-PGC-based Li-DIHSC exhibits excellent EDLC behavior like a Li-HSC in the low-middle wide potential range, and anion intercalation/de-intercalation behavior like a DIB in the high potential range. We find that the Li-DIHSC displays an extremely high energy density of 581 W h kg^{-1}, verifying the performance enhancement by hybridization of the dual-ion battery and hybrid supercapacitor.

Acknowledgments

This work was supported by the National Natural Science Foundation of China (grant no. 51672151).

References

[1] B. Li, J. Zheng, H. Zhang, L. Jin, D. Yang, H. Lv, C. Shen, A. Shellikeri, Y. Zheng, R. Gong, Adv Mater. 30 (2018) 1705670.
[2] H. Wang, C. Zhu, D. Chao, Q. Yan, H.J. Fan, Adv Mater. (2017) 29.
[3] X. Yu, C. Zhan, R. Lv, Y. Bai, Y. Lin, Z.-H. Huang, W. Shen, X. Qiu, F. Kang, Nano Energy. 15 (2015) 43–53.
[4] J. Yang, X. Xiao, P. Chen, K. Zhu, K. Cheng, K. Ye, G. Wang, D. Cao, J. Yan, Nano Energy. 58 (2019) 455–465.
[5] C. Zhan, W. Liu, M. Hu, Q. Liang, X. Yu, Y. Shen, R. Lv, F. Kang, Z.-H. Huang, NPG Asia Mater. 10 (2018) 775–787.
[6] P. Jeżowski, O. Crosnier, E. Deunf, P. Poizot, F. Béguin, T. Brousse, Nat. Mater. 17 (2017) 167.
[7] I.A. Rodríguez-Pérez, X. Ji, ACS Energy Lett. 2 (2017) 1762–1770.
[8] S. Rothermel, P. Meister, G. Schmuelling, O. Fromm, H.-W. Meyer, S. Nowak, M. Winter, T. Placke, Energy Environ. Sci. 7 (2014) 3412–3423.
[9] P. Meister, O. Fromm, S. Rothermel, J. Kasnatscheew, M. Winter, T. Placke, Electrochim Acta 228 (2017) 18–27.
[10] X. Yu, J. Lu, C. Zhan, R. Lv, Q. Liang, Z.-H. Huang, W. Shen, F. Kang, Electrochim Acta 182 (2015) 908–916.
[11] F. Zhang, B. Ji, X. Tong, M. Sheng, X. Zhang, C.-S. Lee, Y. Tang, Adv Mater. Interfaces 3 (2016) 1600605.
[12] X. Gao, C. Zhan, X. Yu, Q. Liang, R. Lv, G. Gai, W. Shen, F. Kang, Z.-H. Huang, Materials (Basel) 10 (2017) 414.
[13] Q. Liang, L. Ye, Z.-H. Huang, Q. Xu, Y. Bai, F. Kang, Q.-H. Yang, Nanoscale 6 (2014) 13831–13837.
[14] Y. Lei, Z.-H. Huang, Y. Yang, W. Shen, Y. Zheng, H. Sun, F. Kang, Sci. Rep. 3 (2013) 2477.
[15] L. Ye, Q. Liang, Y. Lei, X. Yu, C. Han, W. Shen, Z.-H. Huang, F. Kang, Q.-H. Yang, J. Power Sources 282 (2015) 174–178.
[16] C. Zhan, X. Yu, Q. Liang, W. Liu, Y. Wang, R. Lv, Z.-H. Huang, F. Kang, RSC Adv. 6 (2016) 89391–89396.
[17] X. Yu, J.-g. Wang, Z.-H. Huang, W. Shen, F. Kang, Electrochem Commun. 36 (2013) 66–70.
[18] H. Liu, S. Li, H. Yang, S. Liu, L. Chen, Z. Tang, R. Fu, D. Wu, Adv Mater. 29 (2017) 1700723.
[19] C.-H. Huang, Q. Zhang, T.-C. Chou, C.-M. Chen, D.S. Su, R.-A. Doong, ChemSusChem 5 (2012) 563–571.
[20] G. Yang, H. Han, T. Li, C. Du, Carbon N. Y. 50 (2012) 3753–3765.
[21] Y. Liang, W. Zhang, D. Wu, Q.-Q. Ni, M.Q. Zhang, Adv Mater. Interfaces 5 (2018) 1800430.
[22] J.-G. Wang, H. Liu, H. Sun, W. Hua, H. Wang, X. Liu, B. Wei, Carbon N.Y. 127 (2018) 85–92.